The Fornax Deep Survey (FDS) photometric catalog

Abstract

We present the catalog of *ugri*-bands photometry and morphometry for ~1.7 million sources over the ~21 square degree area of the Fornax deep survey (FDS) centered on the bright central galaxy NGC 1399. For a wider area, of ~27 square degrees extending in the direction of NGC 1316, we provide *gri* photometry for ~3.1 million sources. FDS is a survey carried out with the OMegaCAM camera on the VST telescope, and is a joint project that used the GTO time of NOVA (PI. R.F. Peletier) and the INAF survey VEGAS (PI. M. Capaccioli & E. Iodice). To improve the morphological characterization of sources, we generated multi-band image stacks by coadding the best-seeing *gri*-band single exposures with a cut at full width at half maximum FWHM≤0.9 arcsec. The final catalog contains: (i) source identification and position from the multi-band stacks; (ii) the calibrated and aperture corrected AB magnitudes derived from PSF photometry in all available bands; (iii) the uncorrected aperture and Kron-like magnitudes in all bands; (iv) the morphometric parameters (FWHM, CLASS_STAR, concentration index, flux radius, elongation and sharpness) for the multi-band stacks, as well as the latter for all other available bands. In addition to the photometry for the data available in the FDS image repository, the present release contains images and weight maps for the FDS field n. 8. The reference publication, with all the required details on the present catalog, is Cantiello et al. (2020, A&A 639, A136).

Overview of Observations

The imaging data of the FDS survey, already available as ESO Phase3 products, were obtained with OmegaCAM/VST in *u, g, r*, and *i* bands. The footprint of the catalog is given in Figure 1.
In addition to the images released from the survey, for the present catalog we generated multi-band stacks by coadding the best-seeing *gri*-band single exposures with a cut at full width at half maximum FWHM≤0.9 arcsec (referred as *a*-stacks in the following), used as master detection frames to allow a more robust identification of compact sources. Moreover, images and weight maps of the field n. 8 are also used, and made available through the ESO Phase3 archive.

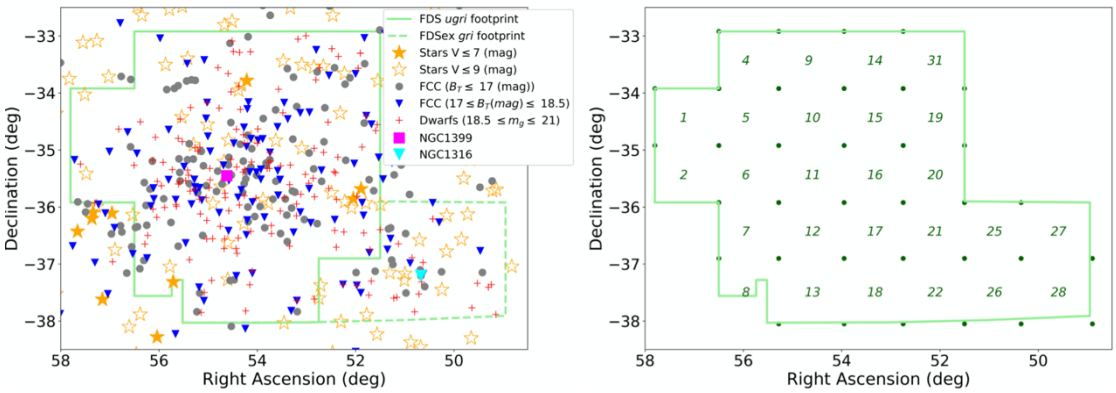

Figure 1. Left panel: FDS footprint of the area covered by ugri photometry (green solid line), and by only gri (dashed green line). Other sources from catalogs available in the literature are also shown, as labeled. Bright galaxies from the Fornax Cluster Catalog (Ferguson, 1989) are subdivided into two categories: likely members brighter than B_T = 17 mag and with 17 ≤ B_T (mag) ≤ 18.5 (filled gray circles and blue triangles, respectively; from Ferguson 1989, Table II). Dwarf galaxies from FDS by Venhola et al. (2018), in the magnitude range 18.5 ≤ m_g (mag) ≤ 21, are indicated with red crosses. The positions of the two brightest galaxies, NGC 1316 and NGC 1399, are also shown with a filled cyan triangle and a magenta square, respectively. Orange filled or empty five-pointed stars mark those stars with m_V ≤ 7/≤9 mag, respectively. Right panel: FDS and FDS-extended area. Green lines mark the edges of the survey, green bullets show the edges of single pointing; the ID of the field is also indicated.

Release Content

The ~21 sq. deg. *ugri* imaging data of FDS centered on NGC 1399 (Fig. 1, solid green line in the left panel), and the additional ~6 sq. deg. *gri* observations in the direction of NGC 1316 (dashed lines in the left panel of Fig. 1, referred as FDS-extended, FDSex, area), have the image quality parameters specified in Table 1. In the table we report the median FWHM, principal colors (linear combinations of colors of stars, P_2-related columns in Tab. 1, for more details see Ivezić et al., 2004), and limiting magnitudes for point sources and for all available bands and fields. We calibrate our photometry to the AB system.

The final catalog contains: (i) source identification adopting the IAU naming rules and position from the *a*-stacks; (ii) the calibrated and aperture corrected AB magnitudes from PSF photometry derived with DAOphot in all available bands; (iii) the uncorrected aperture and Kron-like magnitudes from SExtractor; (iv) the morphometric parameters for *a*-stacks (FWHM, CLASS_STAR, concentration index, flux radius, elongation and sharpness), as well as items *(iii)* and *(iv)* for all other available bands.

The complete catalog contains 50 (41) different photometric and morphometric parameters for the ~1.7 (~3.1) million sources with *ugri* (*gri*) photometry detected in the FDS(ex) area, excluding large diffuse galaxies presented elsewhere in the FDS series. The data volume is ~1.2 GB for the photometric catalogue, 1.0 GB for the images and 6.6 GB for the weighting maps.

Table 1. Image quality parameters for FDS and FDSex fields.

Field ID	$FWHM_u$ ($''$)	$FWHM_g$ ($''$)	$FWHM_r$ ($''$)	$FWMH_i$ ($''$)	$FWHM_a$ ($''$)	$\langle P_2(s)\rangle$ (mag)	$\sigma[P_2(s)]$ (mag)	$\langle P_2(w)\rangle$ (mag)	$\sigma[P_2(w)]$ (mag)	$\langle P_2(x)\rangle$ (mag)	$\sigma[P_2(x)]$ (mag)	$u_{\rm lim}$ (mag)	$g_{\rm lim}$ (mag)	$r_{\rm lim}$ (mag)	$i_{\rm lim}$ (mag)
(1)	(2)	(3)	(4)	(5)	(6)	(7)	(8)	(9)	(10)	(11)	(12)	(13)	(14)	(14)	(16)
1	1.17 ± 0.03	1.35 ± 0.12	1.14 ± 0.11	0.69 ± 0.08	0.72 ± 0.08	0.006	0.019	0.018	0.024	0.014	0.030	24.24 ± 0.13	25.39 ± 0.10	24.65 ± 0.17	24.53 ± 0.15
2	1.21 ± 0.08	1.11 ± 0.16	0.89 ± 0.05	0.79 ± 0.09	0.79 ± 0.04	0.008	0.018	0.011	0.020	0.005	0.032	24.02 ± 0.18	25.41 ± 0.13	25.04 ± 0.12	24.12 ± 0.13
4	1.19 ± 0.05	1.39 ± 0.13	1.19 ± 0.09	0.70 ± 0.07	0.71 ± 0.07	0.007	0.020	0.052	0.026	−0.005	0.029	24.12 ± 0.09	25.35 ± 0.10	24.65 ± 0.11	24.44 ± 0.14
5	1.35 ± 0.07	1.17 ± 0.14	0.98 ± 0.06	1.11 ± 0.16	0.82 ± 0.09	0.005	0.018	0.007	0.024	0.012	0.033	24.05 ± 0.17	25.48 ± 0.10	24.72 ± 0.08	23.88 ± 0.10
6	1.13 ± 0.07	0.83 ± 0.04	1.08 ± 0.12	1.24 ± 0.14	0.80 ± 0.05	0.005	0.021	0.023	0.023	−0.007	0.033	24.22 ± 0.10	25.70 ± 0.10	24.66 ± 0.14	23.51 ± 0.09
7	1.03 ± 0.06	0.82 ± 0.04	0.90 ± 0.07	1.44 ± 0.13	0.78 ± 0.08	0.007	0.022	0.012	0.020	0.008	0.026	24.16 ± 0.12	25.79 ± 0.11	24.91 ± 0.13	23.35 ± 0.11
8	1.21 ± 0.10	0.93 ± 0.16	0.90 ± 0.12	0.96 ± 0.18	0.84 ± 0.13	0.006	0.021	0.022	0.024	−0.015	0.033	24.23 ± 0.21	25.50 ± 0.22	24.99 ± 0.21	23.72 ± 0.20
9	1.42 ± 0.08	1.20 ± 0.07	0.97 ± 0.08	0.84 ± 0.07	0.82 ± 0.05	0.003	0.022	0.036	0.021	−0.015	0.035	23.96 ± 0.09	25.50 ± 0.12	25.06 ± 0.13	24.38 ± 0.13
10	1.34 ± 0.06	1.15 ± 0.05	0.96 ± 0.07	1.09 ± 0.11	0.86 ± 0.05	0.000	0.018	0.009	0.014	−0.010	0.026	24.09 ± 0.10	25.52 ± 0.09	24.84 ± 0.11	23.96 ± 0.11
11	1.27 ± 0.06	1.09 ± 0.14	1.08 ± 0.14	1.17 ± 0.10	0.84 ± 0.08	0.011	0.023	0.025	0.024	−0.002	0.032	24.09 ± 0.13	25.22 ± 0.10	24.65 ± 0.11	23.64 ± 0.09
12	1.18 ± 0.08	0.80 ± 0.04	0.97 ± 0.07	1.17 ± 0.09	0.80 ± 0.05	0.014	0.024	0.022	0.021	0.001	0.037	24.30 ± 0.09	25.74 ± 0.11	24.85 ± 0.11	23.61 ± 0.09
13	1.10 ± 0.05	0.91 ± 0.05	1.03 ± 0.08	1.16 ± 0.07	0.89 ± 0.05	0.003	0.016	0.021	0.016	−0.003	0.029	24.39 ± 0.18	25.72 ± 0.13	24.99 ± 0.12	24.22 ± 0.13
14	1.46 ± 0.09	1.18 ± 0.09	0.96 ± 0.08	0.85 ± 0.06	0.83 ± 0.06	0.004	0.019	0.012	0.017	0.005	0.028	23.99 ± 0.08	25.43 ± 0.12	24.94 ± 0.13	24.30 ± 0.12
15	1.30 ± 0.05	1.13 ± 0.04	0.88 ± 0.04	0.98 ± 0.09	0.81 ± 0.06	0.001	0.020	0.008	0.022	−0.001	0.031	24.19 ± 0.11	25.37 ± 0.09	25.10 ± 0.08	24.02 ± 0.16
16	1.31 ± 0.04	1.26 ± 0.08	0.91 ± 0.08	1.09 ± 0.07	0.84 ± 0.05	0.008	0.025	0.006	0.020	−0.000	0.035	24.16 ± 0.11	25.31 ± 0.08	24.93 ± 0.11	23.88 ± 0.09
17	1.27 ± 0.06	1.25 ± 0.16	0.82 ± 0.05	1.01 ± 0.07	0.80 ± 0.04	−0.006	0.020	0.020	0.020	−0.011	0.032	24.17 ± 0.09	25.16 ± 0.18	25.21 ± 0.11	24.01 ± 0.10
18	1.12 ± 0.08	0.94 ± 0.05	1.03 ± 0.07	1.12 ± 0.12	0.87 ± 0.09	−0.002	0.018	0.021	0.016	0.007	0.025	24.19 ± 0.23	25.57 ± 0.13	24.93 ± 0.12	24.14 ± 0.13
19	1.26 ± 0.05	1.14 ± 0.09	0.89 ± 0.05	0.86 ± 0.06	0.79 ± 0.05	0.010	0.022	0.042	0.022	0.009	0.025	24.10 ± 0.11	25.46 ± 0.09	25.15 ± 0.10	24.13 ± 0.13
20	1.30 ± 0.05	1.23 ± 0.06	0.92 ± 0.09	1.08 ± 0.08	0.81 ± 0.08	0.019	0.033	−0.006	0.032	0.002	0.044	24.12 ± 0.11	25.17 ± 0.12	24.76 ± 0.13	23.80 ± 0.12
21	1.22 ± 0.05	1.12 ± 0.06	0.78 ± 0.05	0.88 ± 0.08	0.78 ± 0.04	0.001	0.022	0.004	0.027	0.002	0.035	24.06 ± 0.11	25.22 ± 0.09	24.92 ± 0.12	24.22 ± 0.09
22	…	1.03 ± 0.06	0.80 ± 0.06	0.85 ± 0.05	0.79 ± 0.05	…	…	0.004	0.019	0.007	0.029	…	25.27 ± 0.14	24.92 ± 0.13	24.21 ± 0.10
25	…	1.12 ± 0.05	0.76 ± 0.06	0.85 ± 0.08	0.78 ± 0.08	…	…	0.016	0.025	−0.003	0.031	…	25.36 ± 0.11	24.98 ± 0.12	24.10 ± 0.10
26	…	0.95 ± 0.12	0.80 ± 0.04	0.91 ± 0.08	0.78 ± 0.04	…	…	0.037	0.021	−0.018	0.035	…	24.79 ± 0.15	25.00 ± 0.11	23.94 ± 0.13
27	…	1.05 ± 0.09	0.78 ± 0.06	0.89 ± 0.09	0.77 ± 0.08	…	…	0.012	0.026	−0.007	0.042	…	25.19 ± 0.11	24.79 ± 0.15	23.75 ± 0.16
28	…	1.09 ± 0.07	0.79 ± 0.15	0.91 ± 0.11	0.78 ± 0.10	…	…	0.007	0.035	0.013	0.032	…	25.11 ± 0.13	24.65 ± 0.19	23.78 ± 0.14
31	1.46 ± 0.08	1.22 ± 0.06	1.00 ± 0.07	0.86 ± 0.08	0.84 ± 0.05	0.012	0.022	0.030	0.023	0.003	0.032	23.83 ± 0.11	25.31 ± 0.11	24.78 ± 0.15	24.05 ± 0.17
Median	1.26 ± 0.11	1.12 ± 0.15	0.92 ± 0.11	0.94 ± 0.17	0.80 ± 0.04	0.006	0.021	0.017	0.022	0.000	0.032	24.12 ± 0.13	25.38 ± 0.17	24.92 ±0.17	24.02 ± 0.24

Release Notes

Data Reduction and Calibration

The data, data acquisition and reduction procedures are presented in a number of papers of the FDS series (Iodice et al. 2016, 2017a,b, 2019; Venhola et al. 2017, 2018, 2019). The fine tuning of the astrometric calibration is obtained by first associating the source lists extracted from the science images with the 2 Micron All-Sky Survey Point Source Catalog (2MASS PSC; Cutri et al. 2003). A full description of the observations and the pipeline used for data reduction (AstroWISE; McFarland et al. 2013) steps are given in the cited papers.

Here, we describe two critical differences with respect to previous works, specifically related to the focus on compact stellar systems in the present work.

Multi-band *a*-stacks

We generated a new set of master-detection frames, *a*-stacks, to improve the detection and characterization of compact sources. The *a*-stacks are obtained by combining in a single coadded image all single VST exposures in *g*, *r* and *i* bands with a median FWHM≤0.9 arcsec. The combined image

was processed as the single band images, except for the photometric calibration which is not derived. With this procedure, a new frame with narrower and more stable FWHM compared with *ugri* bands is obtained, and used as master detection frame. This improved both the uniformity of detections over the different FDS fields, and the determination of the morphological properties of the sources, allowing more accurate characterization of compact and point-like objects.
The *a*-stacks have a median FWHM smaller by ~15% and with a *rms* scatter a factor of ~2.5 lower than the median and *rms* of the FWHM for the best passband. In general, the depth of the coadded multiband *a*-stack does not change much compared with the best band of the field, because the reduced number of exposures used is compensated by the better S/N due to the higher spatial resolution. The spatial resolution, however, is in all cases enhanced, as shown in the $FWHM_a$ column in Table 1.

Two-steps calibration
Catalogs were extracted independently for each FDS pointing and for each filter, using the *a*-stacks as detection maps; the identification of fields with available data is shown in the right panel of Fig. 1. By construction, the catalogs of each pointing have no overlapping regions. To increase the contrast of faint sources close to the cores of extended galaxies, before running the procedures to obtain the photometry and the morphometry we modeled and subtracted all Fornax members brighter than B_T~18 mag.
To obtain the photometry of sources in FDS frames, we used a combination of procedures, based on SExtractor (Bertin & Arnouts 1996) and DAOphot (Stetson 1987) runs, and newly developed code described in Cantiello et al. (2020, A&A 639, A136) and below for completeness. The galaxy-subtracted frames used in this stage are already calibrated as described in the previous works of the FDS series (see below).
First, we used SExtractor to obtain the mean properties of each frame, like the FWHM; the reference morphometry for each source is obtained from the *a*-stacks, though we also derived the morphometric properties for all available passbands. Then, DAOphot is run on the *a*-stacks, and fed to our procedure to identify bright, non-saturated and isolated stars needed to obtain a variable PSF model over the single pointing. Typically a total of 50 to 100 point-like sources was adopted to model the PSF with DAOphot for each filter and field. The list of PSFs was then fed to DAOphot for PSF modeling, adopting the variable PSF option. The first complete DAOphot run was on the *a*-stack, adopting a 2-sigma threshold above the local background. The output table for this run was used to (i) identify sources to define a master detection catalog, (ii) obtain the DAOphot sharpness parameter that will be used as additional parameter for selecting candidate compact sources.
The master detection catalog was then given as input to run DAOphot on each available filter and for all fields: *ugri* for the FDS area, *gri* for FDSex. We also run SExtractor on the full set of images, to obtain the aperture magnitude (MAG_APER) and the automated aperture magnitude (MAG_AUTO), with the respective photometric errors[1]. For the aperture magnitudes, after some tests we adopted the eight-pixel diameter (~1.7 arcsec).
The photometric calibration is carried out in two steps. The first is the same described in Venhola et al. (2018) and in the release description of the first data release of the FDS images, and uses standard star fields observed each night and comparing their OmegaCAM magnitudes with the final data from the Sloan Digital Sky Survey Data III (Alam et al. 2015). With such calibration, after applying the field and pass-band dependent aperture corrections, the photometry of the same sources in different adjacent FDS pointings showed a spatially variable offset, with a median upper limit of ~0.1 mag. Hence, as a second step of the photometric calibration, to improve the photometric uniformity and consistency over the FDS (and FDSex) area, and to derive the spatially and filter dependent aperture correction maps, we compared our VST photometry of bright non-saturated point-like sources to the APASS photometry and obtained the two-dimensional map that best matches the two datasets. The correction maps are derived from 200 to 300 stars per FDS field, Figure 2 shows an example of correction maps derived for the field FDS#19. Each correction map is then applied to its specific field and passband, to correct the photometry of all sources detected in the specific FDS pointing.

[1]For SExtractor runs, we adopted Gaussian convolution kernels of different sizes depending on the FWHM of the field.

Because APASS lacks *u* coverage, for such passband we adopted a slightly different re-calibration strategy. After the preliminary calibration described above, the *B*-band magnitudes of stars from APASS were transformed to *u*-band using Lupton (2005) transformation equations available from the SDSS web pages. In particular, we used: $u = B_{APASS} + 0.8116 \times (u - g)_{fit} - 0.1313$, where the $(u - g)_{fit}$ color index is derived from the APASS $(g - i)$ and $(g - r)$ indices, using a second degree polynomial fit derived from SDSS data over different sky regions. From this stage on, by using the *u*-band magnitudes of stars in APASS derived as a function of the *B, g, r,* and *i* photometry, we may proceed to derive and apply the *u*-band correction maps as in *gri* bands.

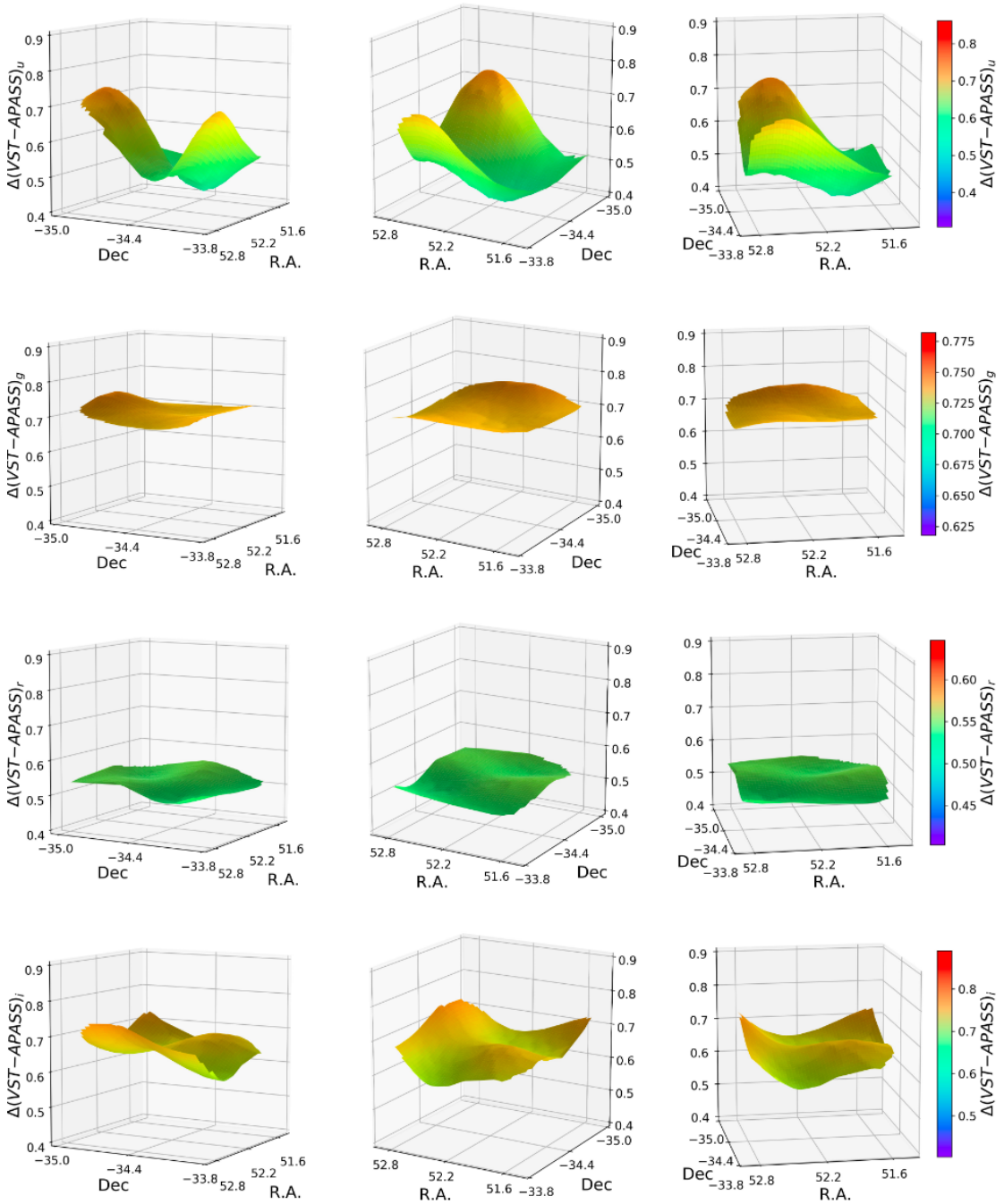

Figure 2. Example of the two-dimensional photometric correction maps for refining the photometry of FDS fields. The maps also include the aperture correction term. Field FDS#19 is shown: u, g, r, and i-band correction maps are plotted from upper to lower panels, respectively.

The magnitudes in the final catalog are not corrected for Galactic extinction, but we include one column with the *E(B-V)* extinction correction, assuming the Galactic extinction values from the Schlafly & Finkbeiner (2011) recalibration of the Schlegel et al. (1998) infrared based dust maps.

To further verify the validity of the calibration obtained with the strategy delineated above, especially for the more elaborate *u*-band, we matched and compared our photometry to the SkyMapper (SM) data (e.g., Wolf et al. 2018). The SDSS photometric systems of APASS and SM are not equivalent, the *u* and *g* bands, in particular, show differences of up to 0.5 mag in the two systems. However, within the color interval $|g - i| \leq 1$ mag, the SM to SDSS difference for *uri*-bands is $\lesssim$0.1 mag, while it is a factor of ~4 larger in *g*-band (see Wolf et al. 2018, their Fig. 17 and Sects. 2.2, 5.4). Hence, as a further consistency check, we compared our VST re-calibrated photometry to SM data, within the color interval $|g - i| \leq 1$ mag.
Over the entire FDS area covered with *ugri* observations, we found ~46 500 sources in common with SM. After identifying bright and isolated stars, and with the given prescriptions on $(g - i)$ color selection, the final sample contains ~4600 objects (~220 per FDS field). The median magnitude offsets between the FDS and SM photometry for the matched sources, is generally good, with the only not unexpected exception of the *g*-band. We find good agreement between the *u, r* and *i* photometry, with magnitude offsets better than 0.02 mag in *r* and *i* bands and of ~0.05 mag in *u*; the *rms* is ~0.03 in *gri* and about twice larger in *u*-band.
For an independent check of the *g*-band photometry, we used the data from the HST/ACS Fornax Cluster Survey (ACSFCS; Jordán et al. 2007, 2015). We matched the ~6300 globular cluster candidates from the ACSFCS with the FDSex *gri* catalog. Adopting a matching radius of 1.0 arcsec, a total of 3750 sources are found in both catalogs. The completeness of the matching is ~90% or higher at bright magnitudes ($m_g \leq 23$ mag), decreases to ~80% for $m_g \leq 24$ mag, and is lower than ~70% for $m_g \leq 25$ mag. Hence, the completeness of the gri catalog drops quickly below $m_g \sim 24.5$ mag, which corresponds to ~0.5 mag fainter than the turn over magnitude (TOM) of the globular cluster luminosity function for galaxies in Fornax (Villegas et al. 2010).
From the matched catalog, we find the median difference is consistent with zero – Δg(FDS – ACSFCS)= – 0.03 ± 0.12 mag for the full sample of 3750 matched sources; Δg(FDS – ACSFCS)= – 0.01 ± 0.07 mag for the 1455 sources in the reference catalog – with no evidence of significant residual trends.

Data Quality

Table 1 provides collection of data quality checks and parameters derived from the FDS catalog.

As an overall photometric quality assessment, we used principal colors, described in Ivezić et al. (2004). Principal colors are linear combinations of the SDSS colors of stars. We adopted the coefficients and selection parameters given in Tables 1–3 of Ivezić et al. (2004). The colors are combined to obtain a new color perpendicular to the stellar locus. Assuming the position of the locus to be fixed, the value of the principal colors is then an internal measure of the absolute photometric calibration of the data. Table 1 provides the median and *rms* width of three principal colors, P_2(s), P_2(w) and P_2(x) for each FDS field; the median P_2 values over the full set of fields is < 0.02 mag with *rms* $\lesssim$ 0.03 mag. The P_2(s) depends on the *u*-band photometry, and cannot be determined over the FDSex fields. The overall $\langle P_2 \rangle$ and $\sigma[P_2]$ values, and the values for each field, are consistent with the same value reported by Ivezić et al. (2004) for SDSS.
Finally, we obtain the limiting magnitudes reported in Table 1 for all fields and bands, derived as 5σ magnitude integrated over the PSF, determined from the median S/N estimated as Δm_{PSF}^{-1}. The median *g*-band limiting magnitude is $g_{lim} \sim 25.4 \pm 0.2$ mag; we note that the faintest globular clusters matched with the ACSFCS reach $g_{lim} \sim 25.6$ mag, which increases to $g_{lim} \sim 25.2$ mag for the sources in the reference catalog.

Known issues

-

Previous Releases

With the present catalogue release, we complement the FDS imaging data of DR1 with the *ugri* observations of the FDS field n. 8.

Data Format

Files Types

The whole catalog is provided as a FITS table, together with the *ugri* FITS images and weigh maps of the field n. 8. All relevant information for the catalog and images is in the file header.

Catalogue Columns

	Label	Format	Unit	Description
1	ID	String	"	Source ID based on the IAU naming
2	RA	Double	deg	Right ascension (J2000.0)
3	Dec	Double	deg	Declination (J2000.0)
4	mu	Double	mag	u-band PSF corrected magnitude
5	emu	Double	mag	error on u-band PSF corrected magnitude
6	mg	Double	mag	g-band PSF corrected magnitude
7	emg	Double	mag	error on g-band PSF corrected magnitude
8	mr	Double	mag	r-band PSF corrected magnitude
9	emr	Double	mag	error on r-band PSF corrected magnitude
10	mi	Double	mag	i-band PSF corrected magnitude
11	emi	Double	mag	error on i-band PSF corrected magnitude
12	CLASS_STAR	Double	"	SExt. CLASS_STAR from the multi-band a-stacks
13	Conc_indx	Double	"	Normalized concentration index from a-stacks
14	Flux_Rad	Double	arcs	SExt. Flux radius from the multi-band a-stacks
15	FWHM	Double	arcs	Source FWHM from the multi-band a-stacks
16	Major_axis	Double	deg	SExt. Profile RMS along major axis - a-stacks
17	Minor_axis	Double	deg	SExt. Profile RMS along minor axis - a-stacks
18	Elongation	Double	"	Elongat., major-to-minor axis ratio - a-stacks
19	Flags	Long	"	Flags, based on SExt. flags coding rules
20	Sharpness	Double	"	DAOphot sharpness parameter from the a-stacks
21	CLASS_STAR_u	Double	"	SExt. CLASS_STAR - u-band
22	Conc_indx_u	Double	"	Normalized concentration index - u-band
23	Sharpness_u	Double	"	DAOphot sharpness parameter - u-band
24	mu8pix	Double	mag	Aperture magnitude within 8 pixels - u-band
25	emu8pix	Double	mag	Error on Aperture mag. within 8 pix. - u-band
26	muauto	Double	mag	SExt. automated apert. mag. MAG_AUTO - u band
27	emuauto	Double	mag	Error on automated ap. mag. MAG_AUTO - u band
28	CLASS_STAR_g	Double	"	SExt. CLASS_STAR - g-band
29	Conc_indx_g	Double	"	Normalized concentration index - g-band
30	Sharpness_g	Double	"	DAOphot sharpness parameter - g-band
31	mg8pix	Double	mag	Aperture magnitude within 8 pixels - g-band
32	emg8pix	Double	mag	Error on Aperture mag. within 8 pix. - g-band
33	mgauto	Double	mag	SExt. automated apert. mag. MAG_AUTO - g band
34	emgauto	Double	mag	Error on automated ap. mag. MAG_AUTO - g band
35	CLASS_STAR_r	Double	"	SExt. CLASS_STAR - r-band
36	Conc_indx_r	Double	"	Normalized concentration index - r-band
37	Sharpness_r	Double	"	DAOphot sharpness parameter - r-band
38	mr8pix	Double	mag	Aperture magnitude within 8 pixels - r-band
39	emr8pix	Double	mag	Error on Aperture mag. within 8 pix. - r-band
40	mrauto	Double	mag	SExt. automated apert. mag. MAG_AUTO - r band
41	emrauto	Double	mag	Error on automated ap. mag. MAG_AUTO - r band
42	CLASS_STAR_i	Double	"	SExt. CLASS_STAR - i-band
43	Conc_indx_i	Double	"	Normalized concentration index - i-band
44	Sharpness_i	Double	"	DAOphot sharpness parameter - i-band
45	mi8pix	Double	mag	Aperture magnitude within 8 pixels - i-band
46	emi8pix	Double	mag	Error on Aperture mag. within 8 pix. - i-band
47	miauto	Double	mag	SExt. automated apert. mag. MAG_AUTO - i band

48	emiauto	Double	mag	Error on automated ap. magn. MAG_AUTO - i band
49	ebv	Double	mag	Reddening from Schlafly & Finkbeiner (2011)
50	FDSfield	Long	"	FDS field pointing ID

Acknowledgements

The FDS Catalog was produced by Michele Cantiello(1) within the FDS collaboration, Enrichetta Iodice (PI,2), Reynier Peletier (PI,3), Massimo Capaccioli (Former PI, 4), Aku Venhola (5), Raffaele D'Abrusco (6), Jesús Falcón- Barroso (7,8), Aniello Grado (2), Michael Hilker (9), Luca Limatola(2), Steffen Mieske (10), Nicola Napolitano (2,11), Maurizio Paolillo (2,4), Marilena Spavone (2), Edwin Valentijn (3), Glenn van de Ven (12), Gijs Verdoes Kleijn (3)

(1) INAF Astronomical Observatory of Abruzzo, via Maggini, I-64100, Teramo, Italy
(2) INAF Astronomical Observatory of Capodimonte, Salita Moiariello 16, I80131, Naples, Italy
(3) Kapteyn Institute, University of Groningen, Landleven 12, 9747 AD Groningen, the Netherlands
(4) University of Naples Federico II, C.U. Monte Sant'Angelo, Via Cinthia, 80126 Naples, Italy
(5) Astronomy Research Unit, University of Oulu, Pentti Kaiteran katu 1, 90014 Oulu, Fin- land
(6) Center for Astrophysics | Harvard & Smithsonian, 60 Garden Street, 02138 Cambridge, MA, USA
(7) Instituto de Astrofśica de Canarias, Calle Vía Láctea s/n, 38200 La Laguna, Tenerife, Spain
(8) Depto. Astrofísica, Universidad de La Laguna, Calle Astrofísico Francisco Sánchez s/n, 38206 La Laguna, Tenerife, Spain
(9) European Southern Observatory, Karl-Schwarzschild-Str. 2, 85748 Garching bei München, Germany
(10) European Southern Observatory, Alonso de Cordova 3107, Vitacura, Santiago, Chile
(11) School of Physics and Astronomy, Sun Yat-sen University, Zhuhai Campus, 2 Daxue Road, Xiangzhou District, Zhuhai, PR China
(12) Department of Astrophysics, University of Vienna Türkenschanzstraße 17, 1180 Vienna, Austria.

Based on data products created from observations collected at the European Organization for Astronomical Research in the Southern Hemisphere under ESO programs 60.A-9038(A), 088.B-4012(A), 090,B-0414(C), 092.B-0744(D), 094.B-0512(A), 094.B-0512(B), 094.B-0496(A), 096.B-0582(A), 096.B-0501(B), 098.B-0208(A), 098.B-0298(A), 098.B-0298(B), 0100.B-0148(A), 0100.B-0148(B), 0100.B-0168(A).

This research has made use of the services of the ESO Science Archive Facility.